# Room-Temperature Fabricated Amorphous $Ga_2O_3$ High-Response-Speed Solar-Blind Photodetector on Rigid and Flexible Substrates

*Shujuan Cui, Zengxia Mei,* Yonghui Zhang, Huili Liang, and Xiaolong Du**

**A solution to the fabrication of amorphous $Ga_2O_3$ solar-blind photodetectors on rigid and flexible substrates at room temperature is reported. A robust improvement in the response speed is achieved by delicately controlling the oxygen flux in the reactive radio frequency magnetron sputtering process. Temporal response measurements show that the detector on quartz has a fast decay time of 19.1 μs and a responsivity of 0.19 A $W^{-1}$ as well, which are even better than those single crystal $Ga_2O_3$ counterparts prepared at high temperatures. X-ray photoelectron spectroscopy and current–voltage tests suggest that the reduced oxygen vacancy concentration and the increased Schottky barrier height jointly contribute to the faster response speed. Amorphous $Ga_2O_3$ solar-blind photodetector is further constructed on polyethylene naphthalate substrate. The flexible devices demonstrate similar photoresponse behavior as the rigid ones, and no significant degradation of the device performance is observed in bending states and fatigue tests. The results reveal the importance of finely tuned oxygen processing gas in promoting the device performance and the applicability of room-temperature synthesized amorphous $Ga_2O_3$ in fabrication of flexible solar-blind photodetectors.**

## 1. Introduction

Flexible and transparent electronics have been developed with great momentum due to their ubiquitous applications in new electronic technologies, involving wearable energy-harvesting systems, soft portable devices, rollup displays, and paper electronics.[1–3] Flexible thin film transistors,[4] field-effect diodes,[5] nanogenerators,[6] supercapacitors,[7] and photodetectors (PDs)[1,2,8–11] have been consequently exploited to act as building blocks for next generation information and energy technologies. Integration of highly flexible, sensitive, and economic deep UV (DUV) solar-blind (200–280 nm) PDs with other device components will certainly become an important area driven by the research and market as it enables the wearable or portable DUV light monitoring with high signal-to-noise ratio and without affecting the visibility of the integrated system beneath. The robust deformability and cheap cost promise the flexible UV photodetectors versatile applications in portable electronic gadgets and display devices as well as biomedical imaging, etc.

DUV solar-blind PDs are usually constructed on wide band gap semiconductor materials, including diamond,[12] AlGaN,[13,14] MgZnO,[15–17] and $Ga_2O_3$.[18–21] Among them, $Ga_2O_3$ is a desirable candidate because of its cheap cost and suitable wide bandgap (≈4.5–4.9 eV) without the necessity of alloying process,[22,23] which makes it attract more and more attention in recent years. Most of the ever-reported $Ga_2O_3$ PDs are prepared on single-crystal substrates at high temperatures (>800 °C) by complicated processes, metal-organic chemical vapor deposition,[24] molecular beam epitaxy,[25] and pulsed laser deposition[26] techniques for instance. However, flexible devices put limitations on the maximum working temperatures since plastic substrates generally have low glass transition temperatures, typically ≈80–150 °C. Therefore, it is essential to explore compatible low-temperature deposition processes for high-quality flexible $Ga_2O_3$ solar-blind PDs. Moreover, thin-film type $Ga_2O_3$ PDs often demonstrate slow response speed even to a level of seconds, known as persistent photoconductivity (PPC) effect, which is far away from the strict requirement of fast response. In general, PPC in oxide is believed relating with deep traps induced by oxygen vacancy ($V_O$) defects.[27,28] The influence of oxygen atmosphere on device performance and the relevant mechanism has to be considered in the low-temperature deposition process as well. Till date, no reports were available in literature regarding the elaborated study on this issue, more specifically, the effect of fine regulation of oxygen atmosphere on $Ga_2O_3$ PD performance.

Here in this work, a series of amorphous $Ga_2O_3$ films are deposited by radio frequency magnetron sputtering technique at room temperature (RT) under different oxygen fluxes. Sputtering systems are widely used in large-area metal oxide semiconductor deposition, with the merits of low cost, low

S. J. Cui, Prof. Z. X. Mei, Y. H. Zhang, Dr. H. L. Liang, Prof. X. L. Du
Beijing National Laboratory for Condensed Matter Physics
Institute of Physics
Chinese Academy of Sciences
Beijing 100190, P. R. China
E-mail: zxmei@iphy.ac.cn; xldu@iphy.ac.cn
S. J. Cui, Y. H. Zhang, Prof. X. L. Du
School of Physical Sciences
University of Chinese Academy of Sciences
Beijing 100049, P. R. China

DOI: 10.1002/adom.201700454

 

temperature, and scalability. For ease of device fabrication and analysis, influence of oxygen flux on photoresponse properties is first studied on amorphous $Ga_2O_3$ PDs on quartz. All devices show a photoresponse peak below 280 nm, within the solar-blind spectrum region. Unlike the substoichiometric oxygen deficiency changing the optical bandgap,[29] the subtly tuned oxygen flux during sputtering significantly enhances the response speed and a fast decay time of 19.1 µs is hence achieved. X-ray photoelectron spectroscopy (XPS) and current–voltage (*I–V*) tests indicate that the remarkable suppression of PPC effect is owing to the reduction of native oxygen vacancy defects and the increase of Schottky barrier height. Fabrication of devices on flexible polyethylene naphthalate (PEN) substrates is then researched and the flexible PDs basically perform the same as the rigid ones. Meanwhile, the device performance exhibits no obvious degradation in bending and fatigue tests.

## 2. Results and Discussion

Without changing the Ar gas flux (10 standard cubic centimeter per minute (sccm)) and rf power (60 W), the only altered processing condition during the sputtering growth was the oxygen flux, which was 0.12, 0.13, 0.14, and 0.15 sccm, labeled as S1, S2, S3, S4, respectively. The reference sample sputtered at pure Ar atmosphere is named as S0. X-ray diffractometer (XRD, Rigaku SmartLab) was employed to confirm the crystallinity of all the sputtered $Ga_2O_3$ films. **Figure 1**a shows the grazing incidence X-ray diffraction curves of the $Ga_2O_3$ films grown under different oxygen fluxes. There is no signature peak observed except the wide envelope one at about 21.5° originating from amorphous quartz substrate,[30] indicating that the $Ga_2O_3$ films grown at RT are amorphous (a-$Ga_2O_3$). To determine the optical bandgap of these a-$Ga_2O_3$ films, transmittance spectrum was measured by using the Varian Cary 5000 UV–vis spectrophotometer. As exhibited in Figure 1b, the delicate variation of oxygen flux makes little difference to the absorption edge of the films, i.e., the optical bandgap does not change along with the subtly varied oxygen atmosphere in our experiments. It is crucial to keep the chemical stoichiometry and optical bandgap constant, otherwise the photoresponse peak and cutoff wavelength will deviate from our expectations. Besides, all the samples show a high transmittance over 85% above 300 nm and a steep drop below 280 nm, manifesting a strong DUV absorption and capability of solar-blind UV light detection. The absorption edge of the samples is obtained from $(\alpha h\nu)^2$ versus $h\nu$ plots as shown in the inset in Figure 1b, where $\alpha$ and $h\nu$ are the absorption coefficient and photon energy, respectively. By fitting the linear region of all the plots of $(\alpha h\nu)^2$ versus $h\nu$, an optical bandgap of about 5.03 eV is derived for all samples, which is very close to the previously reported values.[25,28]

Metal-semiconductor-metal (MSM) structured PD devices are fabricated on these films, whose schematic diagram is shown in **Figure 2**a. Figure 2b presents the dark *I–V* characteristics of the $Ga_2O_3$ prototype PDs with logarithmic coordinate, and the curves in linear coordinate can be found in Figure S1a (Supporting Information). It can be seen that the indium tin oxide (ITO) electrodes form good Schottky contact on a-$Ga_2O_3$ surface. The dark current at a bias of 10 V reaches 0.2 µA in the detector fabricated with film S0. As oxygen flux increases, the dark current drops significantly, even under picoampere level in the case of S3 and S4. To figure out the main transport process on the ITO/$Ga_2O_3$ interface, it is critical to acquire the value of tunneling-related characteristic energy $E_{00}$,[31–33] which, in turn, assists determining the dependence of Schottky barrier height (SBH) on oxygen flux. The formula of $E_{00}$ can be expressed as

$$E_{00} = (\hbar q/2)(N/m^* \varepsilon_r)^{1/2} \quad (1)$$

where $q$, $N$, $m^*$, and $\varepsilon_r$ denote the elementary charge, carrier concentration, effective mass, and dielectric permittivity, respectively. In our calculation, $m^*$ is taken as $0.34m_0$[34] and $\varepsilon_r = 10$.[35] As for the carrier concentration $N$, it is not easy to get an exact value because the sample's resistivity is too high to be detected in our Hall test system, which is far less than $1 \times 10^{15}$ cm$^{-3}$. $E_{00}$ is therefore estimated smaller than 0.17 meV, i.e., $K_BT \gg E_{00}$. It means that the thermionic

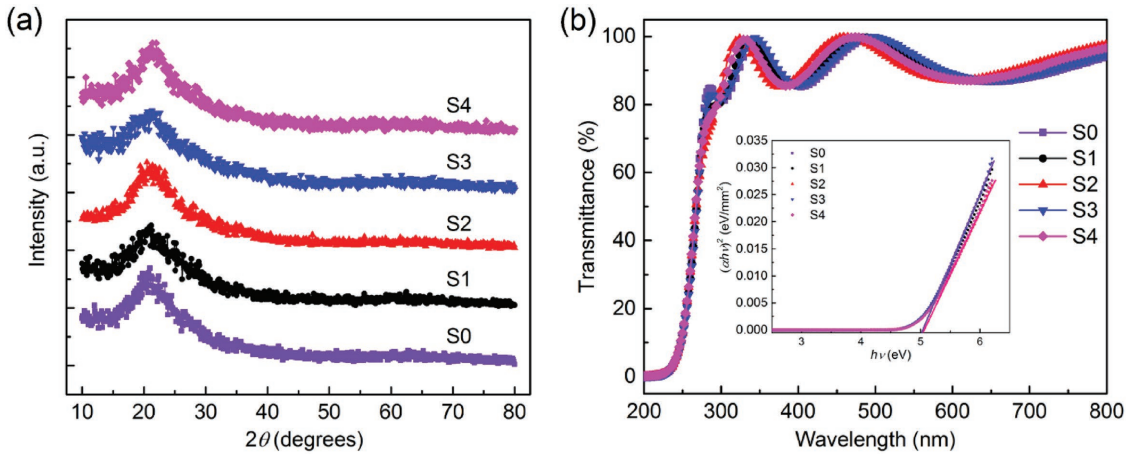


**Figure 1.** a) XRD grazing incidence curves of the amorphous $Ga_2O_3$ films. b) The optical transmittance spectra of the a-$Ga_2O_3$ films. The inset shows the plot of $(\alpha h\nu)^2$ versus $h\nu$ for a-$Ga_2O_3$ films.

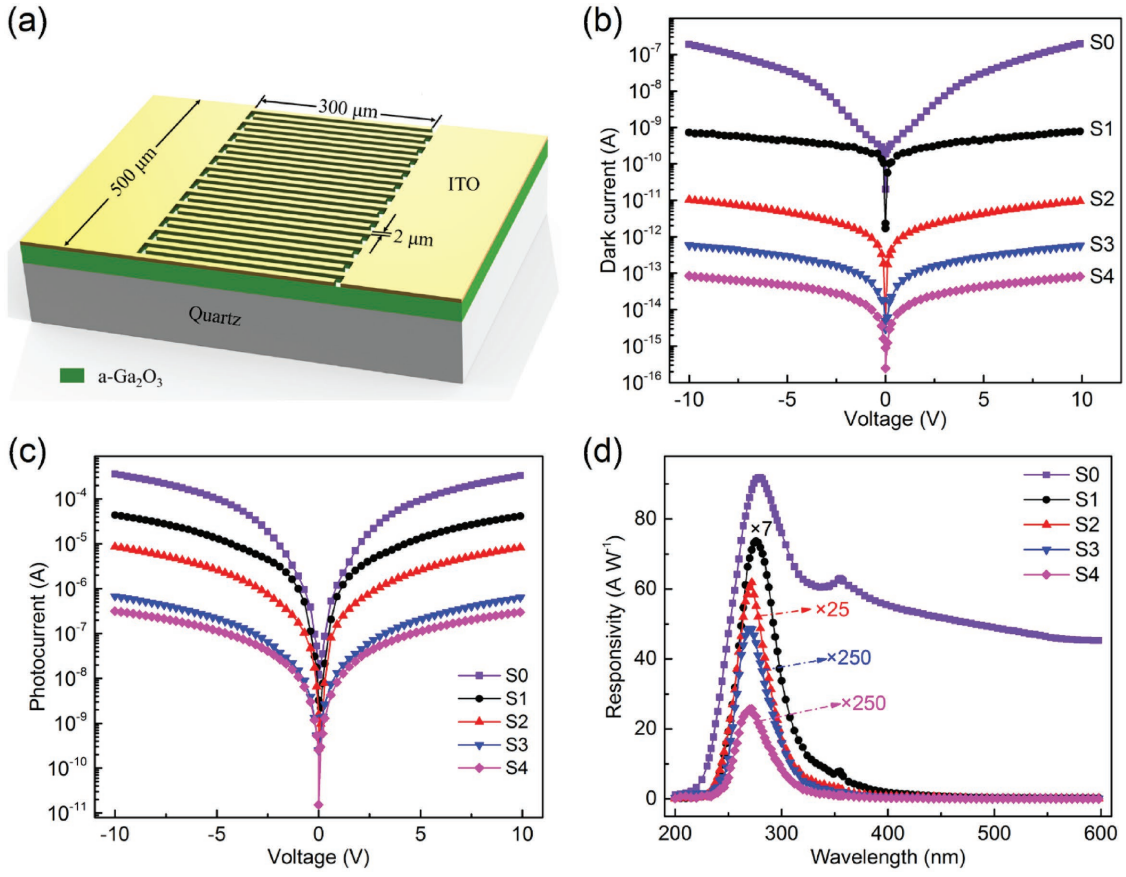


**Figure 2.** a) Schematic diagram of the MSM structure $Ga_2O_3$ PD on quartz. b) *I–V* curves in dark and c) under UV 254 nm light illumination. d) Photoresponsivity spectra of the PDs biased at 20 V.

emission dominates the carrier transport process on the ITO/$Ga_2O_3$ interface.

In general, the current going through the MSM structure with two back to back SBs can be extracted as follows[33]

$$I = I_1\left[\exp\left(\frac{qV}{nK_BT}\right)-1\right]+I_2\left[\exp\left(-\frac{qV}{nK_BT}\right)-1\right] \quad (2)$$

$$I_1 = A_1A_n^*T^2\exp\left(-\frac{q\Phi_{B1}}{K_BT}\right) \quad (3)$$

$$I_2 = A_1A_n^*T^2\exp\left(-\frac{q\Phi_{B2}}{K_BT}\right) \quad (4)$$

where $A_1$ is the junction area and $A_n^*$ is the effective Richardson constant, which is 41 A cm$^{-2}$ K$^{-2}$ for $Ga_2O_3$.[36] $q\Phi_{B1}$ and $q\Phi_{B2}$ are the heights of the two SBs, respectively. Through fitting all the dark *I–V* curves using Equations (2)–(4), the values of the SBH can be derived accordingly (**Table 1**). The fitting curve of S0 can be found in Figure S1b (Supporting Information) as an example. The results show that the SBH gradually increases by ≈0.4 eV from S0 to S4. As there are negative surface defect states in the samples sputtered by the mixture of Ar and $O_2$, they will make the energy band of $Ga_2O_3$ bent upward and further increase the barrier height.[37] Existence of the negative surface states can be deduced from the change of the barrier heights. As can be seen from Table 1, all the samples sputtered with $O_2$ incorporated have relatively asymmetric barriers compared to the pure Ar sputtered S0. The asymmetric barriers indicate the existence of the negative surface states, possibly the oxygen interstitials or absorbed oxygen.[32,37]

Figure 2c gives the *I–V* curves of the PDs under 254 nm UV light illumination. The photoresponse performance of all the a-$Ga_2O_3$ PDs on quartz is listed in **Table 2**. The photocurrent regularly decreases about three order of magnitudes when the

**Table 1.** SBH extracted by fitting the dark *I–V* curves.

| Samples | Oxygen flux [sccm] | At forward bias | | At reverse bias | |
|---|---|---|---|---|---|
| | | $q\Phi_{B1}$ [eV] | $q\Phi_{B2}$ [eV] | $q\Phi_{B1}$ [eV] | $q\Phi_{B2}$ [eV] |
| S0 | 0 | 0.68 | 0.67 | 0.66 | 0.67 |
| S1 | 0.12 | 0.81 | 0.85 | 0.85 | 0.82 |
| S2 | 0.13 | 0.94 | 0.91 | 0.90 | 0.94 |
| S3 | 0.14 | 1.01 | 0.97 | 0.97 | 1.01 |
| S4 | 0.15 | 1.08 | 1.02 | 1.02 | 1.09 |

**Table 2.** The photoresponse performance of a-$Ga_2O_3$ PDs on quartz.

| Samples | Oxygen flux [sccm] | $I_{254}$ @ 10 V bias [A] | Responsivity [A $W^{-1}$] | Decay time—$\tau_d$ [μs] | |
|---|---|---|---|---|---|
| | | | | $\tau_1$ | $\tau_2$ |
| S0 | 0 | $3.36 \times 10^{-4}$ | 91.88 | $1.48 \times 10^6$ | $4.51 \times 10^6$ |
| S1 | 0.12 | $4.14 \times 10^{-5}$ | 12.13 | 123.60 | 853.20 |
| S2 | 0.13 | $8.41 \times 10^{-6}$ | 2.48 | 73.90 | 140.00 |
| S3 | 0.14 | $6.46 \times 10^{-7}$ | 0.19 | 19.10 | 80.70 |
| S4 | 0.15 | $3.05 \times 10^{-7}$ | 0.10 | 42.20 | 80.00 |

oxygen flux increases from 0 to 0.15 sccm. The decrease of the currents both in dark and under UV illumination is ascribed to the increased SBH which will be discussed in detail later. Figure 2d shows the photoresponsivity spectra of the PDs biased at 20 V. It can be seen that S0 has a very large responsivity of 91.88 A $W^{-1}$ at 280 nm and a very long photoresponse tail due to the serious PPC effect which gradually disappears after the incorporation of oxygen processing gas. As for the other samples, the responsivity decreases tremendously from S1 to S4. On the other hand, the photoresponse peak slightly shifts from 275 (S1) to 273 nm (S2) and 271 nm (S3 and S4), all in the solar-blind region. In addition, there is a notable shoulder peak at about 355 nm in S0 and S1. The peak intensity gradually reduces until it disappears with the increase of the oxygen flux, which implies that it comes from an oxygen-related defect. This defect has also been depicted before,[38,39] and Z. Hajnal et al. proved that this gap state is the oxygen vacancy ($V_O$) defect in the second oxygen site (threefold coordinated with three tetrahedral Ga neighbors).[39] Such a $V_O$ defect as a deep donor can contribute to the photoconductivity response and the PPC effect. From the evolution of this shoulder peak, it can be inferred that the concentration of $V_O$ in our samples was effectively controlled by adjusting the oxygen flux during sputtering growth.

In order to verify the response speed and repeatability of the a-$Ga_2O_3$ PDs on quartz, time-dependent response tests with the 254 nm DUV light on and off in turn were performed for five cycles at 10 V bias. As shown in **Figure 3**a, all the devices demonstrate a good cyclicality to the DUV periodic illumination. More importantly, it is very effective to promote the response speed by delicately increasing the oxygen flux. S0 has a severe PPC phenomenon owing to a large quantity of $V_O$ defects inside the film. After introducing trace amounts of oxygen during the sputtering process, only S1 shows a slight PPC trail, and the others demonstrate much sharper falling edge. It should be noted that the light to dark ratio greatly improves due to the effective suppression of the PPC and the dark current. The photocurrent of S0 just falls down about one order of magnitude when the light is turned off. However, all the other four samples have a light to dark ratio of much larger than $10^4$ and surprisingly over $10^6$ for S4.

Furthermore, the temporal response measurement was performed by KrF pulse laser illumination, as shown in Figure 3b and Table 2. The photoresponse decay curves were fitted by adopting a biexponential relation equation with the following expression[40]

$$y = y_0 + y_1 \exp(-t/\tau_1) + y_2 \exp(-t/\tau_2) \quad (5)$$

In this equation, $y_1$ and $y_2$ are both constants, and $\tau_1$ and $\tau_2$ are two time-constants. In decay process, $\tau_1$ is the fast-response component and $\tau_2$ is the slow-response component. For Sample S0, both $\tau_1$ and $\tau_2$ are at a level of seconds, which is too slow to be applied in practical DUV detection. Minutely increasing oxygen flux can greatly reduce the values of $\tau_1$ and $\tau_2$ to a level of microseconds ($\tau_1$ = 19.10 μs and $\tau_2$ = 80.70 μs for S3). The promotion of temporal response speed mainly comes from the reduction of $V_O$ concentration in the film, which will be discussed in detail later. Nevertheless, $\tau_1$ becomes larger on further increasing the oxygen flux from 0.14 to 0.15 sccm, possibly induced by the too high barrier or the scattering of more interstitial oxygen atoms. For a better comparison, some critical parameters are listed in **Table 3**. It can be seen that the film-type MSM structured PDs[25,26,41] usually show a response time at the level of seconds. Low-dimensional nanostructured devices generally have a big gain in responsivity but instead a very slow response speed.[20,21,42] In contrast, the S3 PD herein

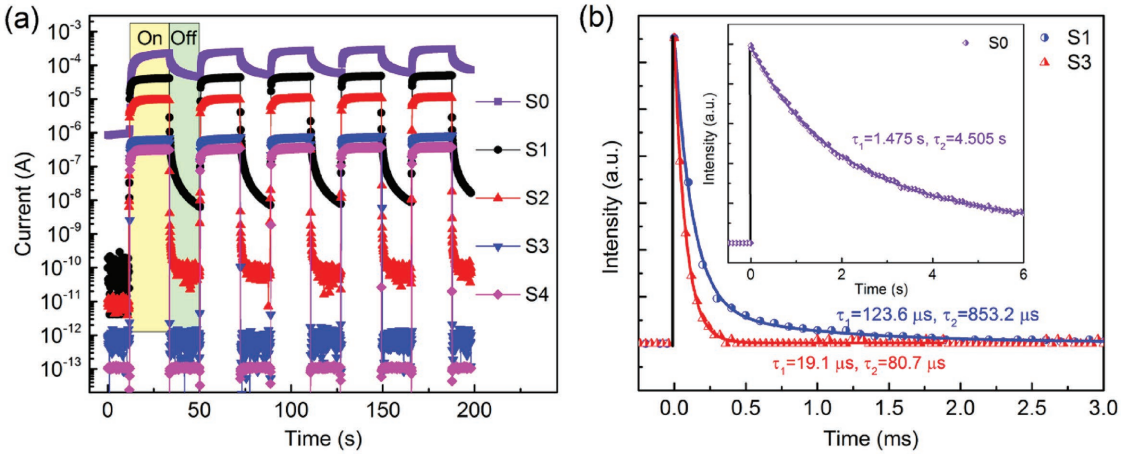


**Figure 3.** a) Time-dependent photoresponse of S0–S4 with the UV 254 nm light on and off at 10V bias. b) Temporal response tests of the PDs with KrF pulse laser illumination at 10 V bias.

**Table 3.** Comparison of the main parameters for the reported $Ga_2O_3$ photodetectors.

| Material | Structure | Responsivity [A W$^{-1}$] | Decay time—$\tau_d$ [μs] | | Reference |
|---|---|---|---|---|---|
| | | | $\tau_1$ | $\tau_2$ | |
| a-$Ga_2O_3$ | Film-based MSM | 0.19 | 19.10 | 80.70 | This work |
| $\beta$-$Ga_2O_3$ | Film-based MSM | – | $1.02\times10^6$ | $1.66\times10^7$ | [25] |
| $\beta$-$Ga_2O_3$ | Film-based MSM | 0.903 | $<3\times10^6$ | | [26] |
| $Ga_2O_3$ | Film-based MSM | 0.037 | – | – | [41] |
| $\beta$-$Ga_2O_3$ | Nanowires | – | $<2\times10^4$ | | [20] |
| $\beta$-$Ga_2O_3$ | Nanobelts | 851 | $<3\times10^5$ | | [21] |
| $\beta$-$Ga_2O_3$ | Micro/nanosheet | 19.13 | $2.30\times10^4$ | | [42] |
| ZnO/$\beta$-$Ga_2O_3$ | Core–shell heterojunction | $1.3\times10^3$ | 42 | 815 | [23] |
| Au/$\beta$-$Ga_2O_3$ | Nanowire array | $6\times10^{-4}$ | 64 | | [43] |

demonstrates a robust improvement in the response speed than previous results. The decay time of 19.1 μs is even much smaller than the recent breakthroughs on $Ga_2O_3$ PDs adopting complex structures, like ZnO/$\beta$-$Ga_2O_3$ core–shell heterojunction[23] or Au/$\beta$-$Ga_2O_3$ nanowire array.[43] Such a fast response speed is significantly meaningful concerning the amorphous film grown at RT and the simple MSM structure.

To further confirm the fine tuning effect of oxygen gas flux in suppressing PPC and enhancing photoresponse speed, XPS analysis was conducted on S0, S1, and S4 samples. In **Figure 4**a, the normalized XPS valence band spectra manifest an obvious shift of the valence band toward the lower binding energy direction, which is very similar to the results of $In_2O_3$ after oxygen plasma treatment.[44] The valence band maximum (VBM) values extracted by the linear extrapolation method are 2.73, 2.49, and 2.28 eV for S0, S1, and S4, respectively. Therefore, the valence band maximum and the conduction band minimum (CBM) bend upward for about 0.45 eV as the oxygen flux increases from 0 to 0.15 sccm, in a good consistence with the results extracted from dark *I*–*V* curves (Table 1). In this case, the SBH between ITO/$Ga_2O_3$ interface also increases which influences the photoelectric behavior of the PDs as shown in Figure 2. For a better understanding, a comparative schematic energy band diagram of S0 and S1–S4 are shown in Figure 4b, respectively. The bandgap ($E_g$) and electron affinity ($\chi$) are taken as 5 and 4 eV[45] for $Ga_2O_3$, respectively, and the work function of ITO is 4.9 eV.[46–48] The Fermi level (zero binding energy in the XPS spectra) of undoped $Ga_2O_3$ is approximately in the middle of the gap. The VBM of S0 locating at 2.73 eV means that the surface energy band bends downward with both VBM and CBM by

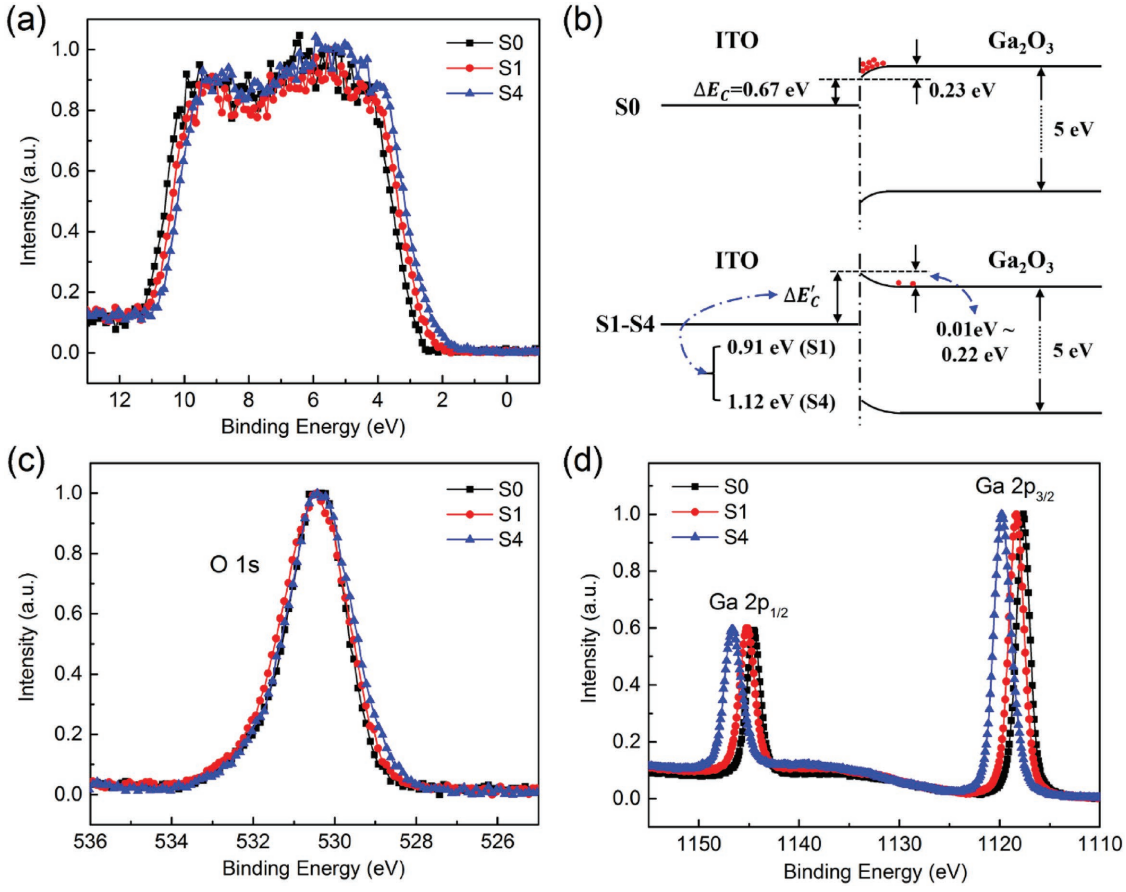


**Figure 4.** a) Normalized XPS valence band spectra of a-$Ga_2O_3$ films. b) Schematic energy band diagrams of the ITO/$Ga_2O_3$ interface. Normalized O 1s c) and Ga 2p d) XPS spectra of a-$Ga_2O_3$ films.

0.23 eV as shown in Figure 4b. The barrier for electrons ($\Delta E_C$) is about 0.67 eV, very close to the value listed in Table 1. For S1, the valence band edge of 2.49 eV indicates a very small upward bending of 0.01 eV. Further increasing the oxygen flux, a higher upward bending will yield a higher SB ($\Delta E'_C$). For S4, the 2.28 eV value of VBM contributes to the upward bending for about 0.22 eV and a $\Delta E'_C$ of 1.12 eV. Such a high SB will effectively block the photoelectrons transporting from $Ga_2O_3$ into ITO, which reduces both the photocurrent and responsivity of the corresponding PDs. A similar upward bending caused by oxygen plasma treatment has been demonstrated by XPS depth tests.[44]

A detailed XPS spectrum of O 1s and Ga 2p emissions is presented in Figure 4c,d, respectively. All the O 1s peaks locating at about 530.3 eV demonstrate a relatively good single-peak symmetry, which is very different from other oxides with a shoulder at the higher binding energy side. This phenomenon has been evidenced in previous studies.[49] In addition, no significant difference is found in these three samples within the XPS resolution (0.4 eV), which implies a negligible change of the oxygen chemical environment in a-$Ga_2O_3$ sputtered under different oxygen fluxes. As exhibited in Figure 4d, the Ga $2p_{3/2}$ peak moves from 1117.6 to 1119.8 eV by a shift as large as 2.2 eV when subtly increasing oxygen flux from 0 to 0.15 sccm. Such a big shift proves a more adequate oxidation state for gallium atoms in a-$Ga_2O_3$, considering the fact that Ga 2p is more sensitive to the oxidation state. Furthermore, the area ratios below the envelope of O 1s to Ga 2p peak ($S_{O1s}/S_{Ga2p}$) are 0.61, 0.64, and 0.65 for S0, S1, and S4, respectively. The increasing tendency of $S_{O1s}/S_{Ga2p}$ shows a definite increase of oxygen content in the films, i.e., an obvious reduction of oxygen vacancies. As a deep level trapping center, the decreased concentration of oxygen vacancy in a-$Ga_2O_3$ significantly promotes the response speed in several orders of magnitude. Of course, increase of the SBH contributes to a faster separation of the photogenerated electron–hole pairs, which can further reduce the response time. However, the reduction of $V_O$ still plays a key role in suppressing the PPC effect as it is the most intrinsic and remarkable variation in the films by precisely changing the sputtered oxygen flux.

Due to the simple and feasible merits of this growth technique, especially the advantage of room temperature deposition (growth process can be found in the Experimental Section), flexible transparent $Ga_2O_3$ DUV PDs were fabricated on PEN substrates by using the sputtered amorphous film at RT, adopting the sputtering conditions of pure Ar and an oxygen flux of 0.14 sccm named as F0 and F1, respectively. Owing to the limitations of UV exposure accuracy for PEN, the interdigital fingers were 5 μm in width spaced by a 5 μm gap (see the top view microscope image in Figure S2a in the Supporting Information).

Transmittance spectra of the whole devices (including the substrates) are shown in **Figure 5**a, and the inset shows the

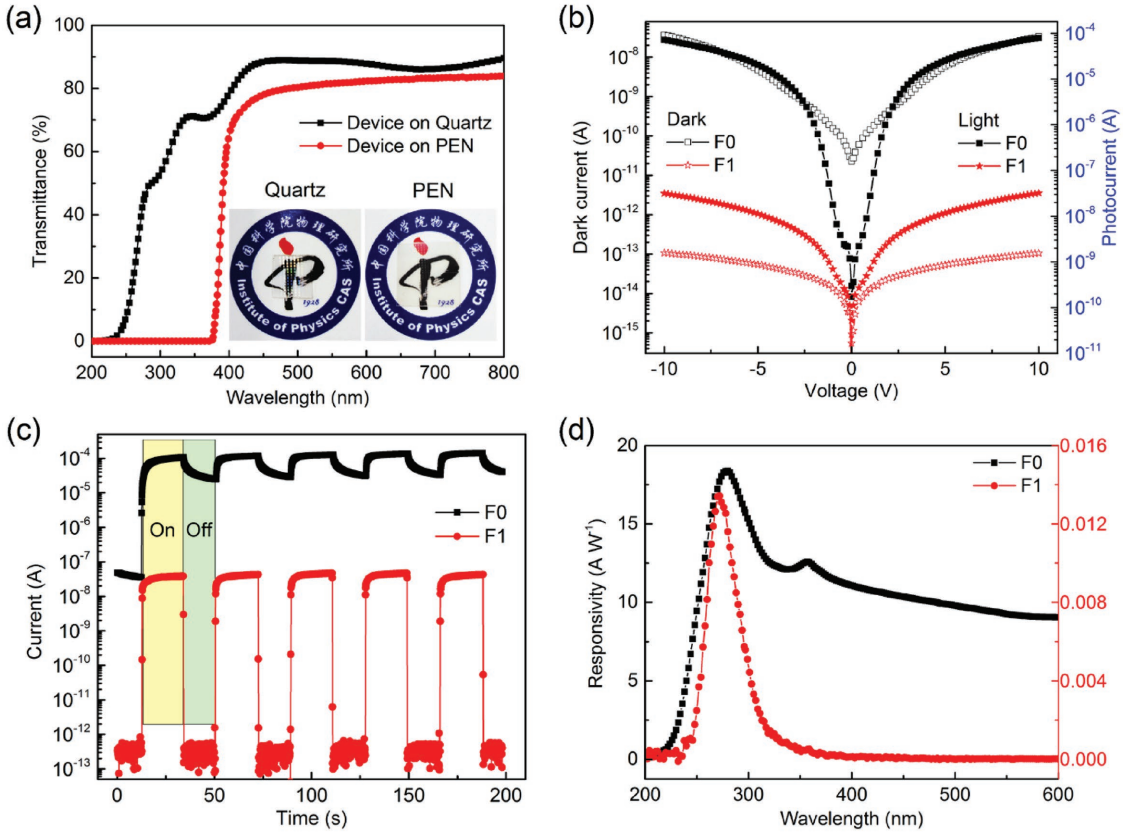


**Figure 5.** a) Optical transmittance spectra of $Ga_2O_3$ PDs on quartz and PEN substrates. b) *I–V* curves of the flexible PDs on PEN substrates tested in dark and under 254 nm illumination. c) Time-dependent photoresponse with the UV 254 nm light on and off. d) Photoresponsivity spectra of flexible PDs F0 and F1.

photographs of two devices on quartz and PEN substrates, respectively. Both of them have a transmittance over 80% in the full visible spectral region (390–780 nm). Figure 5b–d shows the device performance of flexible PDs, F0, and F1, under flat state. Figure 5b gives the *I*–*V* curves in dark and under 254 nm illumination, respectively. The trace amount of oxygen flux affects the currents of flexible devices in the same way as it does in rigid ones (see Figure 2b,c). The time-dependent photoresponse curves with the 254 nm light periodically on and off are illustrated in Figure 5c. A dramatic improvement of the response speed can be seen in F1 when the UV light is turned off. The *I*–*V* curves and time-dependent photoresponse results of rigid devices with the same MSM structure are shown in Figure S2b–d (Supporting Information). Comparing the photoresponse performance of devices on PEN and quartz substrates, we conclude that the flexible devices' performance is basically the same as the rigid ones. Figure 5d presents the photoresponsivity spectra of F0 and F1, where the shoulder peak at around 355 nm in F0 is caused by the oxygen vacancy defects, as R0 in Figure 2d. Definitely, the explored RT deposition process with promoted response speed by delicately adjusting the oxygen flux also works for flexible $Ga_2O_3$ solar-blind PDs.

To investigate the bending influence on photoresponse characteristics of the flexible PDs, the photocurrent–voltage curves, temporal response, and fatigue measurements were carried out in different bent states. **Figure 6**a is a diagrammatic sketch of the flexible device under a bending test and Figure S3 (Supporting Information) shows its in situ photograph. The curved device is considered to be on a circumference of radius *r*, whose value implies the degree of curvature. Photoresponse performances of F1 device at different bending radius *r* were first tested. As shown in Figure 6b,c, the flexible $Ga_2O_3$ PD exhibits almost the same performance under bent states with those on flat state, suggesting a negligible influence of bending stress and satisfying flexibility of these devices. The ignorable difference in these curves may be ascribed to the different contact conditions between the probe and the electrodes when the devices are bent. Figure 6d shows the photocurrent–voltage curves exposed to 254 nm UV light after manually bent 1, 100, 200, and 500 cycles at a curvature degree $r = 8$ mm. The fatigue test presents almost the same curves even after 500 folding cycles. After the fatigue test, the dark current of the device has no obvious degradation, which may be related to the amorphous structure and its antibending and antistretching superiorities. It indicates the flexible $Ga_2O_3$ PD has good robustness and promising applications in the flexible and transparent photoelectronic areas.

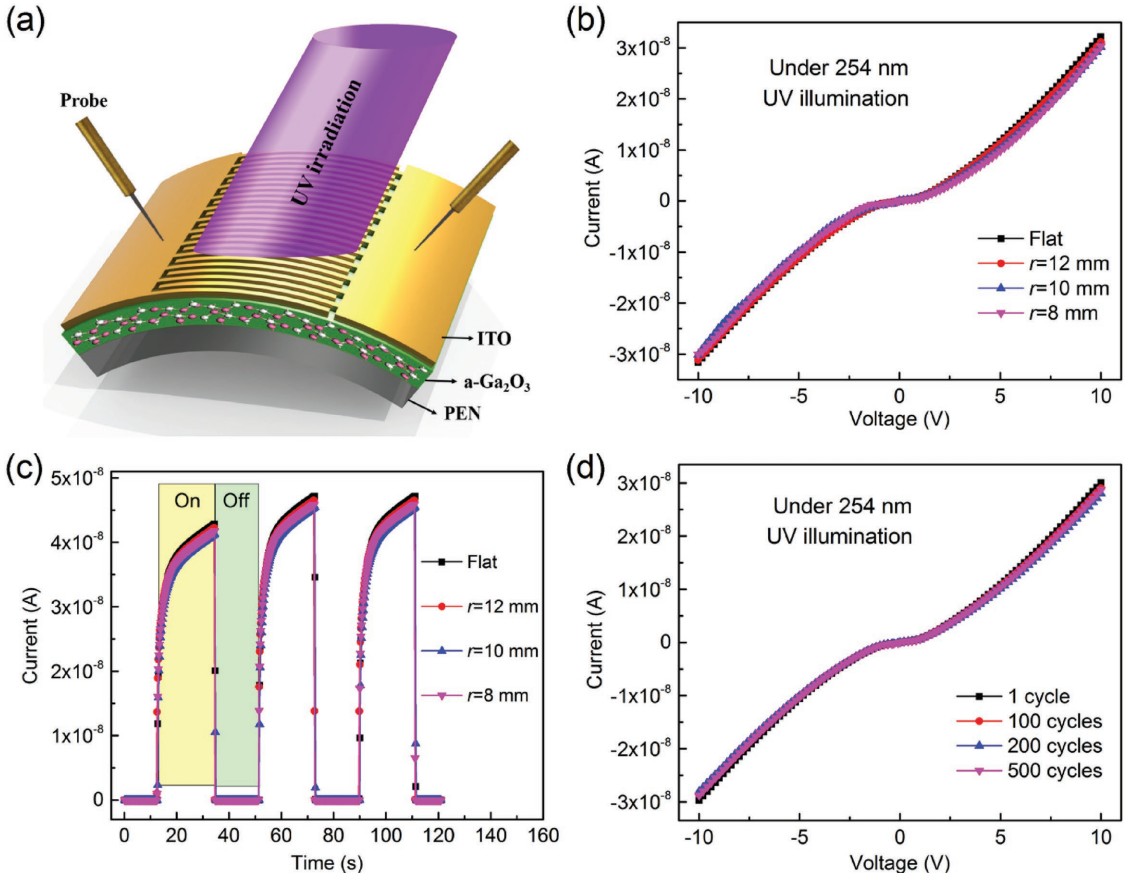


**Figure 6.** a) Schematic diagram of the flexible PD F1 under test while bend. b) Photocurrent–voltage curves of F1 (under 254 nm UV light illumination) under flat and different bending radius. c) Time-dependent photoresponse performance of F1 under flat and different bending radius. d) Photocurrent–voltage curves of F1 exposed to 254 nm UV light illumination after bending 1, 100, 200, and 500 cycles with $r = 8$ mm.

## 3. Conclusion

In summary, deposition of amorphous $Ga_2O_3$ films with finely tuned oxygen vacancy concentration was successfully explored by rf-magnetron sputtering at RT. Fully transparent prototype devices both on quartz and flexible PEN substrates are fabricated with improved solar-blind DUV detection properties, including the photoresponse speed and repeatability. By precisely increasing the oxygen flux in sputtering process, the concentration of oxygen vacancy defects in the films would decrease accordingly and negative surface states generate at the same time. In addition, a higher Schottky contact barrier has been introduced on the ITO/$Ga_2O_3$ interface. Both the reduction of $V_O$ concentration and the increase of SBH result in a greatly enhanced response speed. A much higher light to dark ratio (>$10^4$) and faster decay time of 19.1 μs have been achieved by delicately regulating the oxygen flux in the sputtering process. Additionally, flexible devices have compatible performance with the rigid ones, and no significant degradation was observed during bending and fatigue tests. The results reveal the applicability of room-temperature synthesized amorphous $Ga_2O_3$ in fabrication of flexible solar-blind PDs.

## 4. Experimental Section

*Film Growth*: 250 nm $Ga_2O_3$ films as the absorption layer were deposited on quartz (500 μm thick) and PEN (125 μm thick) substrates by radio frequency magnetron sputtering at room temperature (RT). $Ga_2O_3$ ceramic target was 5N pure. The quartz and PEN substrates were ultrasonically cleaned in acetone, alcohol, and deionized water successively and blown dry with nitrogen at last. Before deposition, the vacuum was evacuated to the base pressure of $2.2 \times 10^{-4}$ Pa. The sputtering lasted for 30 min in total (divided into multiple times to prevent the heating up, expansion, and bending of PEN substrates) under a sputtering power of 60 W and a total pressure of 0.4 Pa. The processing atmosphere was mixed with argon (Ar) and oxygen ($O_2$). During the sputtering for all the samples, the flux of Ar was maintained at 10 sccm. The only difference in the growth conditions was the oxygen flux which varied from 0 to 0.15 sccm. Five samples were grown on quartz substrates with the oxygen flux of 0 (pure Ar, S0), 0.12 (S1), 0.13 (S2), 0.14 (S3), and 0.15 sccm (S4). On PEN substrates, only two conditions were adopted, the pure Ar (F0) and an oxygen flux of 0.14 sccm (F1).

*Photodetectors Fabrication*: The $Ga_2O_3$ solar-blind prototype PDs were constructed with a metal–semiconductor–metal structure by conventional UV-lithography and lift-off technology. PDs on quartz substrates have 125 pair fingers with 2 μm in width, 2 μm in spacing gap, and 300 μm in length. However, PDs on flexible PEN substrates only consist of 25 pair electrodes with 5 μm in width spaced by a 5 μm gap and 300 μm in length (see Figure S2a in the Supporting Information) owing to the limitations of UV exposure accuracy. 100 nm ITO was deposited to form the transparent interdigital electrodes.

*Characterization*: Keithley 6487 picoammeter was used as the power supply for most of the electrical characteristic measurements. However, the dark *I–V* tests of some extremely high resistant samples were measured in air using source-measurement unit in Keithley 4200 semiconductor characterization system. *I–V* curves under illumination were performed using a hand-held lamp with 254 nm DUV light as the light source. Photoresponsivity measurements were performed with the Omni-$\lambda$ 180i grating spectrometer. A KrF excimer laser (248 nm) with a pulse width of 20 ns at a repetition rate of 1 Hz was applied as the excitation source during the temporal response measurements, and a digital oscilloscope with a resolution better than 5 ns for data collection.

## Supporting Information

Supporting Information is available from the Wiley Online Library or from the author.

## Acknowledgements

This work was supported by the National Natural Science Foundation of China (Grants Nos. 11674405, 11675280, 11274366, 51272280, and 61306011). S.C. acknowledges support from the Laboratory of Microfabrication in Institute of Physics, Chinese Academy of Sciences.

## Conflict of Interest

The authors declare no conflict of interest.

## Keywords

amorphous, flexible, $Ga_2O_3$, high response speed, solar-blind photodetectors

Received: May 13, 2017
Published online:

[1] A. Manekkathodi, M.-Y. Lu, C. W. Wang, L.-J. Chen, *Adv. Mater.* **2010**, *22*, 4059.
[2] Z. Wang, H. Wang, B. Liu, W. Qiu, J. Zhang, S. Ran, H. Huang, J. Xu, H. Han, D. Chen, G. Shen, *ACS Nano* **2011**, *5*, 8412.
[3] X. Hou, B. Liu, X. Wang, Z. Wang, Q. Wang, D. Chen, G. Shen, *Nanoscale* **2013**, *5*, 7831.
[4] J. Liu, D. B. Buchholz, R. P. H. Chang, A. Facchetti, T. J. Marks, *Adv. Mater.* **2010**, *22*, 2333.
[5] Y. Zhang, Z. Mei, S. Cui, H. Liang, Y. Liu, X. Du, *Adv. Electron. Mater.* **2016**, *2*, 1500486.
[6] J. M. Wu, C. Xu, Y. Zhang, Y. Yang, Y. Zhou, Z. L. Wang, *Adv. Mater.* **2012**, *24*, 6094.
[7] P.-C. Chen, G. Shen, Y. Shi, H. Chen, C. Zhou, *ACS Nano* **2010**, *4*, 4403.
[8] S. Lu, J. Qi, S. Liu, Z. Zhang, Z. Wang, P. Lin, Q. Liao, Q. Liang, Y. Zhang, *ACS Appl. Mater. Interfaces* **2014**, *6*, 14116.
[9] X. Hu, X. Zhang, L. Liang, J. Bao, S. Li, W. Yang, Y. Xie, *Adv. Funct. Mater.* **2014**, *24*, 7373.
[10] W. Tian, C. Zhang, T. Zhai, S.-L. Li, X. Wang, M. Liao, K. Tsukagoshi, D. Golberg, Y. Bando, *Chem. Commun.* **2013**, *49*, 3739.
[11] P. Hu, L. Wang, M. Yoon, J. Zhang, W. Feng, X. Wang, Z. Wen, J. C. Idrobo, Y. Miyamoto, D. B. Geohegan, K. Xiao, *Nano Lett.* **2013**, *13*, 1649.
[12] F. Foulon, P. Bergonzo, C. Borel, R. D. Marshall, C. Jany, L. Besombes, A. Brambilla, D. Riedel, L. Museur, M. C. Castex, A. Gicquel, *J. Appl. Phys.* **1998**, *84*, 5331.
[13] E. Cicek, R. McClintock, C. Y. Cho, B. Rahnema, M. Razeghi, *Appl. Phys. Lett.* **2013**, *103*, 191108.
[14] D. Walker, V. Kumar, K. Mi, P. Sandvik, P. Kung, X. H. Zhang, M. Razeghi, *Appl. Phys. Lett.* **2000**, *76*, 403.
[15] X. Du, Z. Mei, Z. Liu, Y. Guo, T. Zhang, Y. Hou, Z. Zhang, Q. Xue, A. Y. Kuznetsov, *Adv. Mater.* **2009**, *21*, 4625.
[16] Y. N. Hou, Z. X. Mei, H. L. Liang, D. Q. Ye, C. Z. Gu, X. L. Du, *Appl. Phys. Lett.* **2013**, *102*, 153510.
[17] Y. N. Hou, Z. X. Mei, H. L. Liang, C. Z. Gu, X. L. Du, *Appl. Phys. Lett.* **2014**, *105*, 133510.

[18] W.-Y. Kong, G.-A. Wu, K.-Y. Wang, T.-F. Zhang, Y.-F. Zou, D.-D. Wang, L.-B. Luo, *Adv. Mater.* **2016**, *28*, 10725.
[19] Y. Teng, L. X. Song, A. Ponchel, Z. K. Yang, J. Xia, *Adv. Mater.* **2014**, *26*, 6238.
[20] Y. Li, T. Tokizono, M. Liao, M. Zhong, Y. Koide, I. Yamada, J.-J. Delaunay, *Adv. Funct. Mater.* **2010**, *20*, 3972.
[21] R. Zou, Z. Zhang, Q. Liu, J. Hu, L. Sang, M. Liao, W. Zhang, *Small* **2014**, *10*, 1848.
[22] Y. Kokubun, K. Miura, F. Endo, S. Nakagomi, *Appl. Phys. Lett.* **2007**, *90*, 031912.
[23] B. Zhao, F. Wang, H. Chen, Y. Wang, M. Jiang, X. Fang, D. Zhao, *Nano Lett.* **2015**, *15*, 3988.
[24] K.-W. Chang, J.-J. Wu, *Adv. Mater.* **2005**, *17*, 241.
[25] D. Guo, Z. Wu, P. Li, Y. An, H. Liu, X. Guo, H. Yan, G. Wang, C. Sun, L. Li, W. Tang, *Opt. Mater. Express* **2014**, *4*, 1067.
[26] F.-P. Yu, S.-L. Ou, D.-S. Wuu, *Opt. Mater. Express* **2015**, *5*, 1240.
[27] S. Lany, A. Zunger, *Phys. Rev. Lett.* **2007**, *98*, 045501.
[28] X. Z. Liu, P. Guo, T. Sheng, L. X. Qian, W. L. Zhang, Y. R. Li, *Opt. Mater.* **2016**, *51*, 203.
[29] M. D. Heinemann, J. Berry, G. Teeter, T. Unold, D. Ginley, *Appl. Phys. Lett.* **2016**, *108*, 022107.
[30] G. D. Mukherjee, S. N. Vaidya, V. Sugandhi, *Phys. Rev. Lett.* **2001**, *87*, 195501.
[31] L. Liu, Z. Mei, Y. Hou, H. Liang, A. Azarov, V. Venkatachalapathy, A. Kuznetsov, X. Du, *Sci. Rep.* **2015**, *5*, 15516.
[32] D. L. Jiang, L. Li, H. Y. Chen, H. Gao, Q. Qiao, Z. K. Xu, S. J. Jiao, *Appl. Phys. Lett.* **2015**, *106*, 171103.
[33] J. S. Liu, C. X. Shan, B. H. Li, Z. Z. Zhang, C. L. Yang, D. Z. Shen, X. W. Fan, *Appl. Phys. Lett.* **2010**, *97*, 251102.
[34] H. He, R. Orlando, M. A. Blanco, R. Pandey, E. Amzallag, I. Baraille, M. Rérat, *Phys. Rev. B* **2006**, *74*, 195123.
[35] M. Passlack, E. F. Schubert, W. S. Hobson, M. Hong, N. Moriya, S. N. G. Chu, K. Konstadinidis, J. P. Mannaerts, M. L. Schnoes, G. J. Zydzik, *J. Appl. Phys.* **1995**, *77*, 686.
[36] K. Sasaki, M. Higashiwaki, A. Kuramata, T. Masui, S. Yamakoshi, *IEEE Electron Device Lett.* **2013**, *34*, 493.
[37] T. C. Lovejoy, R. Chen, X. Zheng, E. G. Villora, K. Shimamura, H. Yoshikawa, Y. Yamashita, S. Ueda, K. Kobayashi, S. T. Dunham, F. S. Ohuchi, M. A. Olmstead, *Appl. Phys. Lett.* **2012**, *100*, 181602.
[38] G. Schmitz, P. Gassmann, R. Franchy, *J. Appl. Phys.* **1998**, *83*, 2533.
[39] Z. Hajnal, J. Miró, G. Kiss, F. Réti, P. Deák, R. C. Herndon, J. M. Kuperberg, *J. Appl. Phys.* **1999**, *86*, 3792.
[40] Y. Pei, R. Pei, X. Liang, Y. Wang, L. Liu, H. Chen, J. Liang, *Sci. Rep.* **2016**, *6*, 21551.
[41] T. Oshima, T. Okuno, S. Fujita, *Jpn. J. Appl. Phys.* **2007**, *46*, 7217.
[42] M. Zhong, Z. Wei, X. Meng, F. Wu, J. Li, *J. Alloys Compd.* **2015**, *619*, 572.
[43] X. Chen, K. Liu, Z. Zhang, C. Wang, B. Li, H. Zhao, D. Zhao, D. Shen, *ACS Appl. Mater. Interfaces* **2016**, *8*, 4185.
[44] O. Bierwagen, J. S. Speck, T. Nagata, T. Chikyow, Y. Yamashita, H. Yoshikawa, K. Kobayashi, *Appl. Phys. Lett.* **2011**, *98*, 172101.
[45] M. Mohamed, K. Irmscher, C. Janowitz, Z. Galazka, R. Manzke, R. Fornari, *Appl. Phys. Lett.* **2012**, *101*, 132106.
[46] P. J. Hotchkiss, H. Li, P. B. Paramonov, S. A. Paniagua, S. C. Jones, N. R. Armstrong, J.-L. Brédas, S. R. Marder, *Adv. Mater.* **2009**, *21*, 4496.
[47] K. Kikuchi, S. Imura, K. Miyakawa, M. Kubota, E. Ohta, *Thin Solid Films* **2014**, *550*, 635.
[48] S. A. McDonald, G. Konstantatos, S. Zhang, P. W. Cyr, E. J. D. Klem, L. Levina, E. H. Sargent, *Nat. Mater.* **2005**, *4*, 138.
[49] M. Michling, D. Schmeißer, *IOP Conf. Ser.: Mater. Sci. Eng.* **2012**, *34*, 012002.

 